Dong, J., Sun, W., Zhou, X., Wang, R. (2016): An analytical approach to estimate curvature effect of coseismic deformations. - *Geophysical Journal International*, *206*, 2, pp. 1327—1339.

DOI: http://doi.org/10.1093/gji/ggw215

Geophysical Journal International

Geophys. J. Int. (2016) **206,** 1327–1339
Advance Access publication 2016 June 5
GJI Seismology

doi: 10.1093/gji/ggw215

An analytical approach to estimate curvature effect of coseismic deformations

Jie Dong,[1] Wenke Sun,[1] Xin Zhou[1,2] and Rongjiang Wang[3]

[1] *Key Laboratory of Computational Geodynamics, University of Chinese Academy of Sciences, Beijing* 100049, *China. E-mail: dongmei731@163.com*
[2] *Earthquake Research Institute, the University of Tokyo,* 1-1-1 *Yayoi, Bunkyo-ku, Tokyo* 1130032, *Japan*
[3] *GFZ German Research Centre for Geosciences, Telegrafenberg, D*-14473 *Potsdam, Germany*

Accepted 2016 June 2. Received 2016 June 2; in original form 2015 November 24

SUMMARY

We present an analytical approach to compute the curvature effect by the new analytical solutions of coseismic deformation derived for the homogeneous sphere model. We consider two spheres with different radii: one is the same as earth and the other with a larger radius can approximate a half-space model. Then, we calculate the coseismic displacements for the two spheres and define the relative percentage of the displacements as the curvature effect. The near-field curvature effect is defined relative to the maximum coseismic displacement. The results show that the maximum curvature effect is about 4 per cent for source depths of less than 100 km, and about 30 per cent for source depths of less than 600 km. For the far-field curvature effect, we define it relative to the observing point. The curvature effect is extremely large and sometimes exceeds 100 per cent. Moreover, this new approach can be used to estimate any planet's curvature effect quantitatively. For a smaller sphere, such as the Moon, the curvature effect is much larger than that of the Earth, with an inverse ratio to the earth's radius.

Key words: Numerical approximations and analysis; Reference systems; Computational seismology; Theoretical seismology.

1 INTRODUCTION

Dislocation theory for a half-space earth model (Okada 1985) is still often used in computing coseismic displacement, strain and tilt. However, because of its geometrical figure, there is an effect from the earth's curvature and layer structure. Using modern geodetic observation techniques, coseismic deformations can be efficiently observed at a global scale. In this case, the curvature and layer effects should be carefully considered.

For this purpose, some scientists studied coseismic deformations for a spherical model. Ben-Menahem & Singh (1968), Ben-Menahem *et al.* (1969), Singh & Ben-Menahem (1969), Ben-Menahem & Israel (1970) studied coseismic deformation for a homogeneous spherical model without gravity. They claimed that the effect of the earth's curvature is negligible for the near field less than 20°. They did not give a seismic deformation of less than 2° for the difficulty of the numerical calculation. Saito (1967) presented a theory to calculate the amplitudes of free oscillations caused by a point source in a spherically symmetric earth model. He expressed his results in terms of normal mode solutions and source functions, which established a foundation for the spherical dislocation theory. Pollitz (1996) discussed the coseismic deformation, using the normal mode method, of a layered spherical model without gravity. The research revealed that the effect of earth curvature is within 2 per cent when the epicentral distance is less than 100 km. All of these research approaches for a spherical earth are based on the numerical normal mode, but there are accuracy problems due to internal numerical calculation difficulties because it is assumed very limited number of layers (Tanaka *et al.* 2006). Some other scientists (Piersanti *et al.* 1995; Nostro *et al.* 1999; Melini *et al.* 2008) investigated the curvature effect based on an incompressible model, while Nostro *et al.* (1999) studied coseismic and post-seismic surface deformation induced by shear dislocations using flat and spherical earth models. The differences between predictions based on flat and spherical models are because of their global geometry and the effect of the gravity forces.

Wang (1999) proposed an orthonormalization method for stable and efficient computation of Green's functions using a layered half-space model. Wang *et al.* (2003, 2006) further extended the half-space dislocation theory and proposed a series of calculation formulae for the coseismic-gravitational and viscoelastic-gravitational effects, which can be used to calculate Green's functions for all fundamental point sources and any generalized finite-fault source. They considered the layered structures and the gravity effect (Wang 2005), but could not embody the curvature effect.

Sun & Okubo (1993) proposed an approach to compute changes in potential and gravity for a spherical earth model based on 1066A (Gilbert & Dziewonski 1975) model and PREM (Dziewonski & Anderson 1981) model. Sun *et al.* (2009) defined the dislocation Love numbers and Green's functions for four independent sources (strike-slip, dip-slip, horizontal tensile and vertical tensile) to calculate coseismic deformation based on the SNREI earth model. Sun (2003, 2004a,b) also presented asymptotic solutions for calculating deformation in a spherically symmetric Earth. Sun & Okubo (2002) compared the displacements using a homogeneous half-space model, homogeneous spherical model, and studied the curvature and layer effects with an inhomogeneous spherical model. They found that the layer and curvature effects on the coseismic surface deformation (vertical displacement) can reach as large as 25 per cent. However, gravity was included in the spherical earth model computations. On the other hand, their numerical technique results in numerical error in the computed displacements, which affects the investigation of curvature effect.

In this study, we investigate the curvature effect using a new approach, whereby we consider the coseismic displacement for a homogeneous sphere without gravity. First, based on spherical dislocation theory, we derive the analytical solutions of independent point sources for the sphere model. By these analytical solutions, we can calculate any spherical harmonic degrees of the spherical function expressions, without consideration for the truncation error of the infinite series. In this case, the coseismic deformation can be described in analytical expressions. Then, we consider two spheres with different radii so that the larger one can be considered as an approximation of the half-space model. Finally, the curvature effect is obtained by comparing the coseismic displacements obtained for the two spheres. We use the relative percentage of the coseismic displacements to calculate the curvature effect of the earth. Due to the deformation features of the near field and far field, we give different definitions for the curvature effect calculation and present the quantitative estimates, respectively. Above all, by these analytical solutions, we can estimate the curvature effect of any planet, such as the Moon. Dong *et al.* (2014) researched the curvature effect by this method but with some particular assumption, and did not give the detail explanation of this new approach. Also, they had not explored the suitability of this approach for all the planets. Here, we present the complete theory, and improve that work.

2 COSEISMIC DEFORMATION OF A HOMOGENEOUS SPHERE

We consider a homogeneous sphere without gravity. In this case, the coseismic displacement ($\boldsymbol{u}$) and stress ($\boldsymbol{\tau}$) can be expressed in spherical coordinates (r, θ, φ), where r is the radius of the earth and (θ, φ) express the colatitude and longitude, respectively. The deformation is excited by a unit point source ($\boldsymbol{f}$) at a location $(r_0, \theta_0, \varphi_0)$ that satisfies the equations of equilibrium and stress–strain relation (Alterman *et al.* 1959; Takeuchi & Saito 1972). These equations can be written as:

$$\nabla \cdot \boldsymbol{\tau} + \rho \boldsymbol{f} = 0 \tag{1}$$

$$\boldsymbol{\tau} = \lambda \boldsymbol{I} \nabla \cdot \boldsymbol{u} + \mu(\nabla \boldsymbol{u} + (\nabla \boldsymbol{u})^T) \tag{2}$$

where $\boldsymbol{I}$ is the unit tensor, superscript T stands for transpose, μ and λ are the Lame constants of the earth.

Generally, any function can be expressed as spherical harmonics on a unit sphere. To solve eqs (1) and (2), we adopt the vector spherical functions

$$\begin{aligned}
\boldsymbol{R}_n^m(\theta, \varphi) &= \boldsymbol{e}_r Y_n^m(\theta, \varphi) \\
\boldsymbol{S}_n^m(\theta, \varphi) &= \left[\boldsymbol{e}_\theta \frac{\partial}{\partial \theta} + \boldsymbol{e}_\varphi \frac{1}{\sin\theta} \frac{\partial}{\partial \varphi} \right] Y_n^m(\theta, \varphi) \\
\boldsymbol{T}_n^m(\theta, \varphi) &= \left[\boldsymbol{e}_\theta \frac{1}{\sin\theta} \frac{\partial}{\partial \varphi} - \boldsymbol{e}_\varphi \frac{\partial}{\partial \theta} \right] Y_n^m(\theta, \varphi)
\end{aligned} \tag{3}$$

with

$$Y_n^m(\theta, \phi) = P_n^m(\cos\theta) e^{im\phi}, \quad Y_n^{-|m|}(\theta, \phi) = (-1)^m P_n^{|m|}(\cos\theta) e^{-i|m|\phi}, \quad m = 0, \pm 1, \pm 2, \ldots \pm n \tag{4}$$

where $P_n^m(\cos\theta)$ are the associated Legendre's functions. The coseismic displacement $\boldsymbol{u}(r, \theta, \varphi)$ and stress $\boldsymbol{\tau}(r, \theta, \varphi)$ can be expressed as:

$$\boldsymbol{u}(r, \theta, \varphi) = \sum_{n,m} \left[y_1(r) \boldsymbol{R}_n^m(\theta, \varphi) + y_3(r) \boldsymbol{S}_n^m(\theta, \varphi) + y_1^t(r) \boldsymbol{T}_n^m(\theta, \varphi) \right] \tag{5}$$

$$\boldsymbol{\tau} \bullet \boldsymbol{e}_r(r, \theta, \varphi) = \sum_{n,m} \left[y_2(r) \boldsymbol{R}_n^m(\theta, \varphi) + y_4(r) \boldsymbol{S}_n^m(\theta, \varphi) + y_2^t(r) \boldsymbol{T}_n^m(\theta, \varphi) \right] \tag{6}$$

where the superscript t stands for the toroidal deformation. For the spheroidal deformation, y_1 and y_3 are radial and horizontal components of displacement; y_2 and y_4 are radial and horizontal components of stress, while y_1^t and y_2^t are horizontal displacement and stress of toroidal deformation, respectively.

Similarly, a point force $\boldsymbol{f}$ at $(r_0, \theta_0, \varphi_0)$ can be expressed as:

$$\rho \boldsymbol{f} = \frac{\delta(r - r_0)}{r_0^2} \sum_{n,m} \left[F_2(r) \boldsymbol{R}_n^m(\theta, \varphi) + F_4(r) \boldsymbol{S}_n^m(\theta, \varphi) + F_2^t(r) \boldsymbol{T}_n^m(\theta, \varphi) \right] \tag{7}$$

with

$$F_2(r) = \frac{2n+1}{4\pi}\frac{(n-m)!}{(n+m)!}\boldsymbol{R}_n^{m*}(\theta_0,\varphi_0)\cdot\boldsymbol{v}$$

$$F_4(r) = \frac{2n+1}{4\pi n(n+1)}\frac{(n-m)!}{(n+m)!}\boldsymbol{S}_n^{m*}(\theta_0,\varphi_0)\cdot\boldsymbol{v}$$

$$F_2^t(r) = \frac{2n+1}{4\pi n(n+1)}\frac{(n-m)!}{(n+m)!}\boldsymbol{T}_n^{m*}(\theta_0,\varphi_0)\cdot\boldsymbol{v} \tag{8}$$

where * stands for complex conjugate and $\boldsymbol{v}$ is unit vector.

Substituting the formulae (5)–(7) into (1) and (2), and neglecting the gravity effect ($g = 0$), we obtain four ordinary spheroidal differential eq. (9) and two toroidal eq. (10) as:

$$\begin{cases} \frac{dy_1}{dr} = \frac{1}{\beta}\left\{y_2 - \frac{\lambda}{r}\left[2y_1 - n(n+1)y_3\right]\right\} \\ \frac{dy_2}{dr} = \frac{4}{r}\left(\frac{3\kappa\mu}{r\beta}\right)y_1 - \frac{4\mu}{r\beta}y_2 - \frac{n(n+1)}{r}\left(\frac{6\mu\kappa}{r\beta}\right)y_3 + \frac{n(n+1)}{r}y_4 - F_2\frac{\delta(r-r_0)}{r_0^2} \\ \frac{dy_3}{dr} = \frac{1}{\mu}y_4 - \frac{1}{r}(y_1 - y_3) \\ \frac{dy_4}{dr} = -\frac{6\mu\kappa}{r^2\beta}y_1 - \frac{\lambda}{r\beta}y_2 + \left\{\frac{2\mu}{r^2\beta}\left[\left(2n^2+2n-1\right)\lambda + 2\left(n^2+n-1\right)\mu\right]\right\}y_3 - \frac{3}{r}y_4 - F_4\frac{\delta(r-r_0)}{r_0^2} \end{cases} \tag{9}$$

$$\begin{cases} \frac{dy_1^t}{dr} = \frac{1}{r}y_1^t + \frac{1}{\mu}y_2^t \\ \frac{dy_2^t}{dr} = \frac{\mu(n-1)(n+2)}{r^2}y_1^t - \frac{3}{r}y_2^t - F_2^t\frac{\delta(r-r_0)}{r_0^2} \end{cases} \tag{10}$$

where $\beta = \lambda + 2\mu$.

Since we adopt a homogeneous earth model, the general solution ($\boldsymbol{X}$) can be analytically obtained (Love 1911). Although Love (1911) studied this problem, it is difficult to find a suitable solution of $\boldsymbol{X}$ from his publication; therefore, we derive the expressions of $\boldsymbol{X}$ in this study. Omitting the tedious mathematical work, we present four sets of fundamental spheroidal solutions $y_{ji}(i, j = 1, 2, 3, 4)$ and two sets of toroidal solutions $y_{ji}^t(i, j = 1, 2)$.

The spheroidal solutions of the homogeneous equation of (9), including two sets of regular solutions and two sets of irregular solutions, can be obtained analytically:

$$\begin{pmatrix} y_{11}(r) & y_{12}(r) & y_{13}(r) & y_{14}(r) \\ y_{21}(r) & y_{22}(r) & y_{23}(r) & y_{24}(r) \\ y_{31}(r) & y_{32}(r) & y_{33}(r) & y_{34}(r) \\ y_{41}(r) & y_{42}(r) & y_{43}(r) & y_{44}(r) \end{pmatrix}$$

$$= \begin{pmatrix} -(n+1)r^{-n-2} & -\left[\frac{(n+1)\lambda+(n+3)\mu}{(n-2)\lambda+(n-4)\mu}\right]nr^{-n} & \frac{n\lambda+(n-2)\mu}{(n+3)\lambda+(n+5)\mu}(n+1)r^{n+1} & nr^{n-1} \\ 2\mu(n+1)(n+2)r^{-n-3} & \frac{(n^2+3n-1)\lambda+n(n+3)\mu}{(n-2)\lambda+(n-4)\mu}2\mu nr^{-n-1} & \frac{(n^2-n-3)\lambda+(n^2-n-2)\mu}{(n+3)\lambda+(n+5)\mu}2\mu(n+1)r^{n} & 2\mu n(n-1)r^{n-2} \\ r^{-n-2} & r^{-n} & r^{n+1} & r^{n-1} \\ -2\mu(n+2)r^{-n-3} & -\frac{(n^2-1)\lambda+(n^2-2)\mu}{(n-2)\lambda+(n-4)\mu}2\mu r^{-n-1} & \frac{(n^2+2n)\lambda+(n^2+2n-1)\mu}{(n+3)\lambda+(n+5)\mu}2\mu r^{n} & 2\mu(n-1)r^{n-2} \end{pmatrix}. \tag{11}$$

Similarly, the toroidal solutions (one regular solution and one irregular solution) are:

$$\begin{pmatrix} y_{11}^t(r) & y_{12}^t(r) \\ y_{21}^t(r) & y_{22}^t(r) \end{pmatrix} = \begin{pmatrix} r^n & -r^{-(n+1)} \\ \mu(n-1)r^{n-1} & \mu(n+2)r^{-(n+2)} \end{pmatrix}. \tag{12}$$

Then, the general solution ($\boldsymbol{X}$) can be expressed by a combination of the fundamental spheroidal solutions as

$$x_j(r) = \sum_{i=1}^{4}\beta_i y_{ji}(r), \quad j = 1, 2, 3, 4 \tag{13}$$

where β_i are unknown constants. To determine the solution on the earth surface, we introduce the boundary conditions,

$$y_2(r)|_{r=R} = y_4(r)|_{r=R} = 0 \tag{14}$$

$$\boldsymbol{y}_j(r)\big|_{r=r_s^+} - \boldsymbol{y}_j(r)\big|_{r=r_s^-} = \boldsymbol{s}_j, \quad j = 1, 2, 3, 4 \tag{15}$$

$$\boldsymbol{y}(r)|_{r=0} < +\infty \tag{16}$$

where $\boldsymbol{s}$ is seismic source function, which is given by Takeuchi & Saito (1972).

Thus, we may obtain the following equations for the spheroidal solution. Here, we take the vertical strike-slip source as an example:

$$\begin{pmatrix} y_{21}(R) & y_{22}(R) & y_{23}(R) & y_{24}(R) & 0 & 0 \\ y_{41}(R) & y_{42}(R) & y_{43}(R) & y_{44}(R) & 0 & 0 \\ y_{11}(r_s^+) & y_{12}(r_s^+) & y_{13}(r_s^+) & y_{14}(r_s^+) & -y_{13}(r_s^-) & -y_{14}(r_s^-) \\ y_{21}(r_s^+) & y_{22}(r_s^+) & y_{23}(r_s^+) & y_{24}(r_s^+) & -y_{23}(r_s^-) & -y_{24}(r_s^-) \\ y_{31}(r_s^+) & y_{32}(r_s^+) & y_{33}(r_s^+) & y_{34}(r_s^+) & -y_{33}(r_s^-) & -y_{34}(r_s^-) \\ y_{41}(r_s^+) & y_{42}(r_s^+) & y_{43}(r_s^+) & y_{44}(r_s^+) & -y_{43}(r_s^-) & -y_{44}(r_s^-) \end{pmatrix} \begin{pmatrix} \beta_1 \\ \beta_2 \\ \beta_3 \\ \beta_4 \\ \beta_5 \\ \beta_6 \end{pmatrix} = \begin{pmatrix} 0 \\ 0 \\ s_1^{12}(r_s) \\ s_2^{12}(r_s) \\ s_3^{12}(r_s) \\ s_4^{12}(r_s) \end{pmatrix} \tag{17}$$

where R is the radius of the earth and $r_s = (R - r_0)/R$ denotes the normalized radius distance of the source. β_5 and β_6 are unknown constants also. After solving eq. (17), β_i can be determined analytically, but the tedious calculations are not presented. Then, we can obtain the radial and horizontal components of displacement ($y_1^{n,12}(r)$and $y_3^{n,12}(r)$) on the surface.

Similarly, for the toroidal solution, we have:

$$\begin{pmatrix} y_{21}^t(R) & y_{22}^t(R) & 0 \\ y_{11}^t(r_s^+) & y_{12}^t(r_s^+) & -y_{11}^t(r_s^-) \\ y_{21}^t(r_s^+) & y_{22}^t(r_s^+) & -y_{21}^t(r_s^-) \end{pmatrix} \begin{pmatrix} \beta_1^t \\ \beta_2^t \\ \beta_3^t \end{pmatrix} = \begin{pmatrix} 0 \\ s_1^{t,12}(r_s) \\ s_2^{t,12}(r_s) \end{pmatrix}. \tag{18}$$

The unknown constants β_i^t can be obtained in an analytical form as

$$\begin{pmatrix} \beta_1^t \\ \beta_2^t \\ \beta_3^t \end{pmatrix} = \frac{r_s^{n-1}}{8\pi n(n+1)} \begin{pmatrix} \frac{n+2}{n-1} \\ -1 \\ \frac{n+2}{n-1} + {r_s}^{-2n-1} \end{pmatrix}. \tag{19}$$

Then, we obtain the toroidal solution as

$$y_1^{t,n,12}(r) = \frac{r_s^{n-1}}{8\pi n(n+1)} \left(\frac{n+2}{n-1} r^n + r^{-n-1} \right). \tag{20}$$

Similarly, we can obtain the solutions for other sources. Finally, we may compute coseismic displacement $\boldsymbol{u}(r, \theta, \varphi)$ by harmonics summation:

$$\begin{aligned} u_r(r,\theta,\varphi) &= \sum_{n,m} y_{1,m}^n(r) Y_n^m(\theta,\varphi) \cdot r^2 \\ u_\theta(r,\theta,\varphi) &= \sum_{n,m} y_{3,m}^n(r) \frac{\partial Y_n^m(\theta,\varphi)}{\partial\theta} \cdot r^2 + \sum_{n,m} y_{1,m}^{t,n}(r) \frac{1}{\sin\theta} \frac{\partial Y_n^m(\theta,\varphi)}{\partial\varphi} \cdot r^2 \\ u_\varphi(r,\theta,\varphi) &= \sum_{n,m} y_{3,m}^n(r) \frac{1}{\sin\theta} \frac{\partial Y_n^m(\theta,\varphi)}{\partial\varphi} \cdot r^2 - \sum_{n,m} y_{1,m}^{t,n}(r) \frac{\partial Y_n^m(\theta,\varphi)}{\partial\theta} \cdot r^2. \end{aligned} \tag{21}$$

In practical computation, we compute displacement Green's functions on the earth surface ($r = R$). Then, we can obtain the coseismic displacement for a homogeneous spherical earth model without gravity, while considering the dislocation factors.

3 NEW SCHEME TO COMPUTE CURVATURE EFFECT

Sun & Okubo (2002) studied the curvature effect by comparing the difference between a half-space model and a spherical homogeneous sphere. However, in their computing scheme, the gravity effect was involved since Poisson's equation was considered. On the other hand, their numerical method results in computational errors, such as the truncation error of the infinite series. Therefore, we propose a new approach for computing the curvature effect by using the above expressions of coseismic displacement for a homogeneous sphere. We consider two homogeneous spheres with different radiuses (see Fig. 1). The benefit of this scheme is that the same expressions can be used for both spheres and computing error can be undercontrolled. On the other hand, since the computing expressions do not contain gravity, we may obtain a pure curvature effect. The important point is that the difference of two spheres should be large enough for the larger sphere to be equivalent to a half-space within certain epicentral distances.

For example, we assume the earth is a small sphere (the red Sphere 1 in Fig. 1) with the same radius as the earth, and consider a large sphere (the blue Sphere 2 in Fig. 1) with a radius 10 times that of Sphere 1. When the source depths are less than 100 km, the larger sphere is nearly equivalent to a half-space when the spheres have the same source mechanisms (the black star in Fig. 1) at the North Pole. Because Sphere 2 is quite large compared to Sphere 1, the difference between computed coseismic displacements for the two spheres represents the curvature effect.

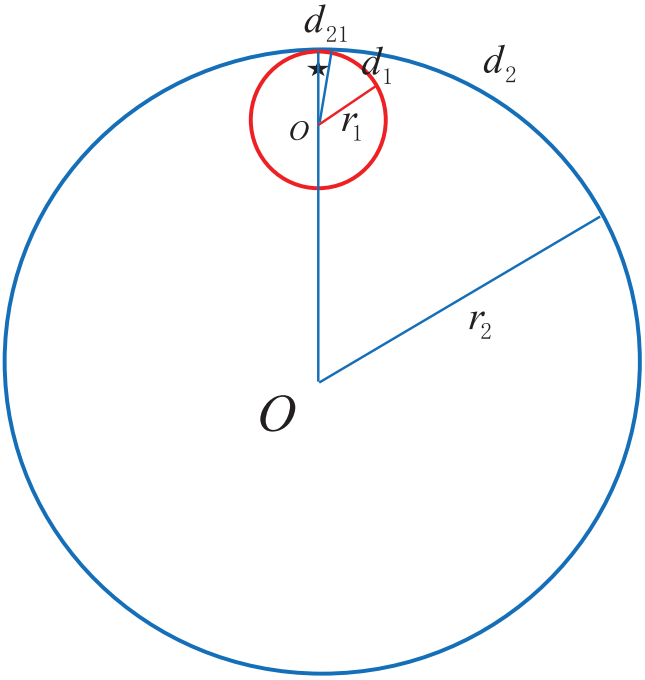

Figure 1. Sketch showing the relationship between Sphere 1 (red sphere) and Sphere 2 (blue sphere), not to scale.

The variables include r_1 and r_2 as the radius of Sphere 1 and Sphere 2, respectively; d_1 is the angular distance of the computing point on Sphere 1; d_2 is the same angular distance as d_1, but on Sphere 2; d_{21} is d_2 corresponding to Sphere 1 (see as eq. 33); and the black star is the point source.

Then, we derive the formulae for computing the curvature effect based on the two spheres. Actually, the coseismic displacement (21) is also a function of source depth (r_0) and angular distance (d), represented as

$$\begin{aligned} u_r(r,\theta,\varphi) &= u_r^{(r)}\left[(r_0,d),\theta,\varphi\right] \\ u_\theta(r,\theta,\varphi) &= u_\theta^{(r)}\left[(r_0,d),\theta,\varphi\right] \\ u_\varphi(r,\theta,\varphi) &= u_\varphi^{(r)}\left[(r_0,d),\theta,\varphi\right]. \end{aligned} \tag{22}$$

For convenience, we denote Green's function as $\boldsymbol{G}$ for a unit point source, so that the coseismic displacement (22) can be expressed by multiplying Green's function by the dislocation factor. The general coseismic displacement at angular distance d can be expressed as

$$\boldsymbol{u}^{(r)}\left[(r_0,d),\theta,\varphi\right] = \frac{M}{\mu r^2}\boldsymbol{G}\left[\left(\frac{r_0}{r},\frac{d}{r}\right),\theta,\varphi\right] \tag{23}$$

where M is the seismic moment and r is the radius of the sphere. Green's function $\boldsymbol{G}[(\frac{r_0}{r},\frac{d}{r}),\theta,\varphi]$ can be used for any sphere with different radius, since $(\frac{r_0}{r},\frac{d}{r})$ is normalized in a unit sphere. Then, we express the displacement caused by the same source, but on different spheres as:

Sphere 1 ($r_1 = R$)

$$\boldsymbol{u}^{(r_1)}\left[(r_0,d),\theta,\varphi\right] = \frac{M}{\mu r_1^2}\boldsymbol{G}\left[\left(\frac{r_0}{r_1},\frac{d}{r_1}\right),\theta,\varphi\right] \tag{24}$$

Sphere 2 ($r_2 = 10R$)

$$\boldsymbol{u}^{(r_2)}\left[(r_0,d),\theta,\varphi\right] = \frac{M}{\mu r_2^2}\boldsymbol{G}\left[\left(\frac{r_0}{r_2},\frac{d}{r_2}\right),\theta,\varphi\right]. \tag{25}$$

Furthermore, we derive the relation between the coseismic displacements for the two spheres as,

$$\begin{aligned} \boldsymbol{u}^{(r_2)}\left[(r_0,d),\theta,\varphi\right] &= \frac{M}{\mu r_2^2}\boldsymbol{G}\left[\left(\frac{r_0\cdot r_1/r_2}{r_1},\frac{d\cdot r_1/r_2}{r_1}\right),\theta,\varphi\right] \\ &= \frac{M}{\mu r_2^2}\cdot\frac{\mu r_1^2}{M}\boldsymbol{u}^{(r_1)}\left[(r_0\cdot r_1/r_2, d\cdot r_1/r_2),\theta,\varphi\right] \\ &= c^2\cdot\boldsymbol{u}^{(r_1)}\left[(r_0\cdot c, d\cdot c),\theta,\varphi\right]. \end{aligned} \tag{26}$$

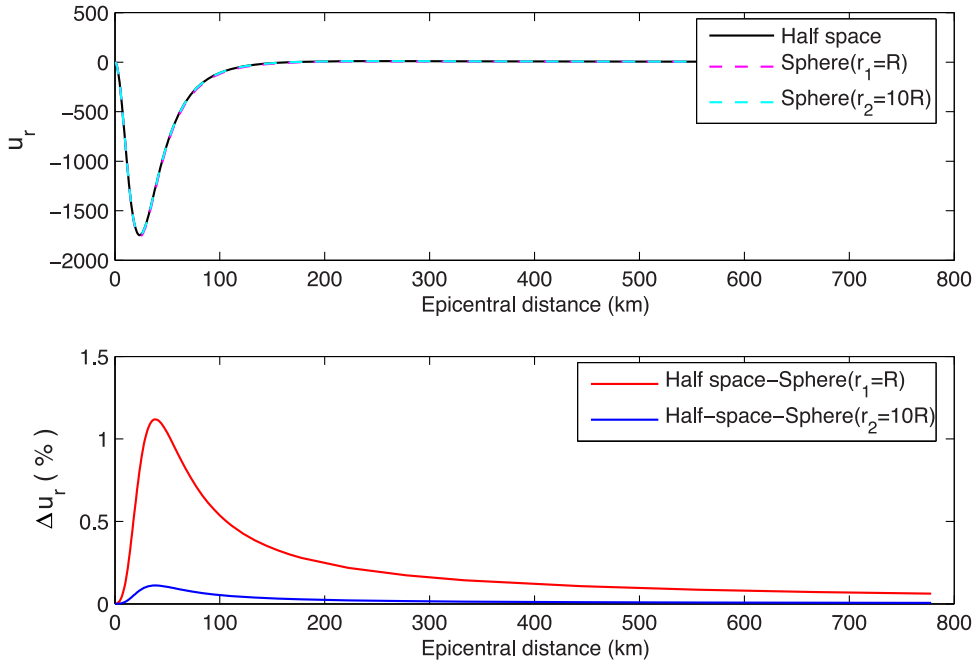

Figure 2. Comparison of the coseismic vertical displacements computed for a half-space, Sphere 1 ($r_1 = R$) and Sphere 2 ($r_2 = 10R$) for a strike-slip point source ($UdS/R^2 = 1$) at a depth of 30 km (the upper panel). The lower panel shows differences of two spheres with respect to the half-space.

Here, $c = r_1/r_2 = 1/10$, then,

$$u_r^{(r_2)}[(r_0, d), \theta, \varphi] = c^2 \cdot u_r^{(r_1)}[(r_0 \cdot c, d \cdot c), \theta, \varphi]$$
$$u_\theta^{(r_2)}[(r_0, d), \theta, \varphi] = c^2 \cdot u_\theta^{(r_1)}[(r_0 \cdot c, d \cdot c), \theta, \varphi]$$
$$u_\varphi^{(r_2)}[(r_0, d), \theta, \varphi] = c^2 \cdot u_\varphi^{(r_1)}[(r_0 \cdot c, d \cdot c), \theta, \varphi]. \quad (27)$$

Since the relation (26) is suitable for any point source, we calculate coseismic displacements using formulae (22) and (27) for Spheres 1 and 2, and compare the difference between them. For Sphere 2, we calculate the displacement using the reformed source and epicentral distance in Sphere 1 by using formula (27).

To confirm the validation of the computing scheme, we compare the coseismic displacements computed for a half-space, Sphere 1 ($r_1 = R$) and Sphere 2 ($r_2 = 10R$), for sources (strike-slip) at depths of 30 and 100 km, respectively, with the results plotted in Figs 2 and 3.

Figs 2 and 3 show that the vertical displacements for half-space and Sphere 2 are quite consistent. The difference between the two models (the blue line of Δu_r) is less than 0.3 per cent. This indicates that the large sphere is nearly equivalent to a half-space for source depths of less than 100 km. On the other hand, the difference of the half-space and Sphere 1 (the red line of Δu_r) is much larger, indicating the curvature effect. In conclusion, the large sphere accurately represents the half-space and can be used to study the curvature effect.

4 CHOICE OF THE LARGE SPHERE

We considered a large sphere with a radius 10 times larger than the small sphere to verify this new method. However, it seems that the larger the radius of the larger sphere, the more accurate the curvature effect so we continue to verify the method by finding the optimal size of the large sphere. We consider several large spheres for comparison and for resolving highly accurate deformation of the large sphere. Assuming a strike-slip source at a depth of 100 km, we compute vertical displacement difference between Half-space and a large sphere with a radius of 5, 10, 20 and 50 times that of R with results illustrated in Fig. 4.

Fig. 4 shows that the differences between half-space model and spheres of $10R$, $20R$ and $50R$ are quite small. A larger radius will result in a smaller difference between the half-space and the sphere. The difference between the half-space and a sphere of $50R$ is nearly zero. From this point of view, the large sphere with a radius of $50R$ is optimal for computing the curvature effect.

Figs 5–7 show that the vertical displacements for half-space and Sphere 2 ($50R$) are nearly the same regardless of shallow source or deep source. We can use the sphere of $50R$ to instead of the half-space to examine the curvature effect.

5 CURVATURE EFFECT ON COSEISMIC DEFORMATIONS

Now we turn to compute the curvature effect by comparing the coseismic displacement $\boldsymbol{u}(r, \theta, \varphi)$ for four independent sources (strike-slip, dip-slip, horizontal tensile and vertical tensile) in homogeneous spheres. The results are shown in Figs 8–11, for sources at 30 and 100 km,

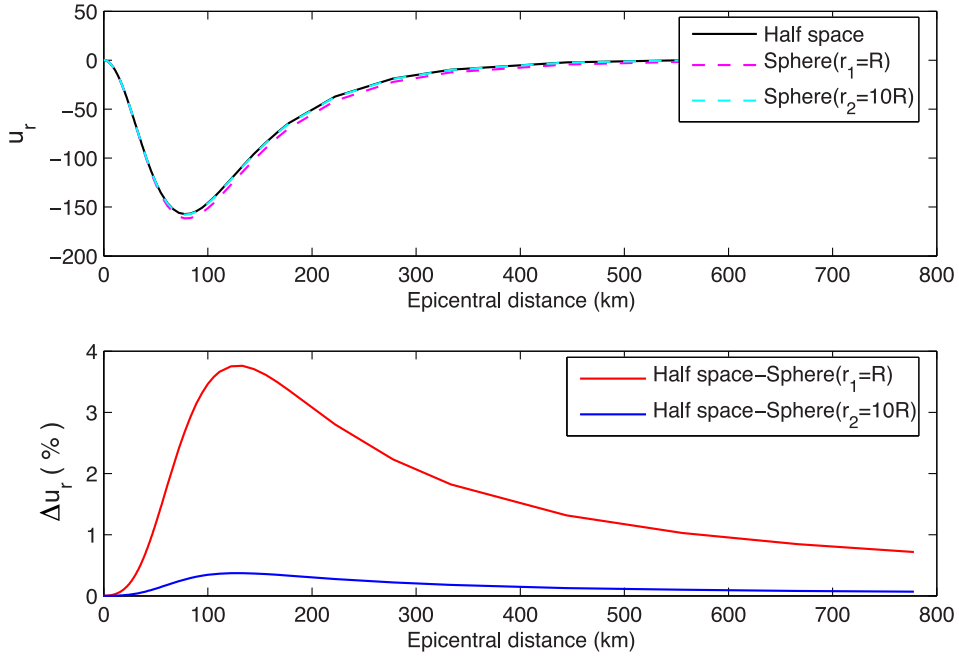

Figure 3. Comparison of the coseismic vertical displacements computed for a half-space, Sphere 1 ($r_1 = R$) and Sphere 2 ($r_2 = 10R$) for a strike-slip point source ($UdS/R^2 = 1$) at a depth of 100 km (the upper panel). The lower panel shows differences of two spheres with respect to the half-space.

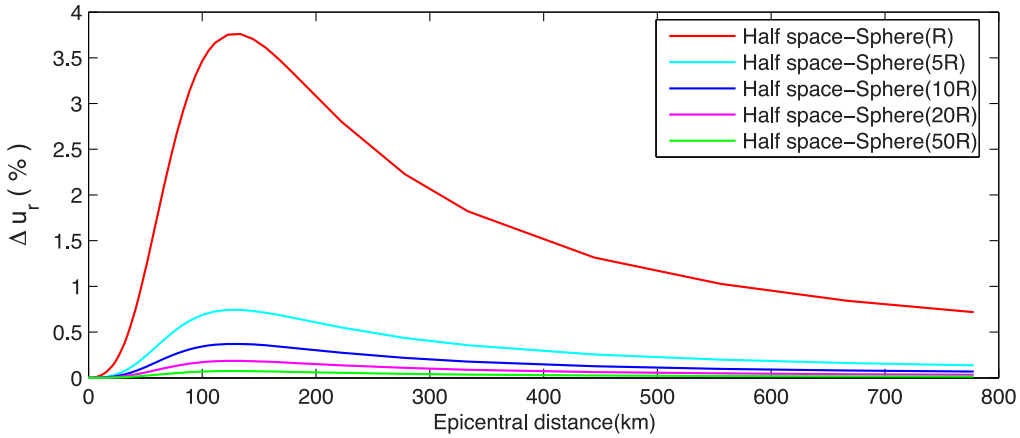

Figure 4. Vertical displacement differences caused by a strike-slip point source (depth = 100 km) between half-space and various large sphere radii.

we take the epicentral distance 770 km. For source depth of 600 km with an epicentral distance of 6600 km. We can estimate the near-field and far-field curvature effect by comparing the coseismic displacements for the two spheres.

5.1 Curvature effect on the near-field deformations

For the near field, quantitative estimates are obtained by defining the curvature effect by the relative error (ε) of the coseismic displacements of the two spheres as

$$\varepsilon = \frac{\left|\boldsymbol{u}^{(r_2)}\right| - \left|\boldsymbol{u}^{(r_1)}\right|}{\left|\boldsymbol{u}^{(r_1)}\right|_{\max}}. \tag{28}$$

The difference of displacements for the two spheres is divided by the maximum displacement on the small sphere.

Results in Figs 8–10 show that the curvature effect varies with the epicentral distance, source type and source depth. The maximum curvature effect occurs at strike-slip shear and horizontal tensile sources, and is also sensitive to source depth. It reaches 1.2 per cent for the source at depth of 30 km (Fig. 8), and about 4.0 per cent for the source at a depth of 100 km (Fig. 9), which is nearly the same as that reported by Dong *et al.* (2014) using the sphere with a radius of $10R$, but a bit smaller. That is because the sphere with a radius of $50R$ is more precise for our research. The curvature effect is as large as 30.0 per cent (Fig. 10) for a strike-slip source of 600 km, while the effect for other three types of sources is about 10 per cent.

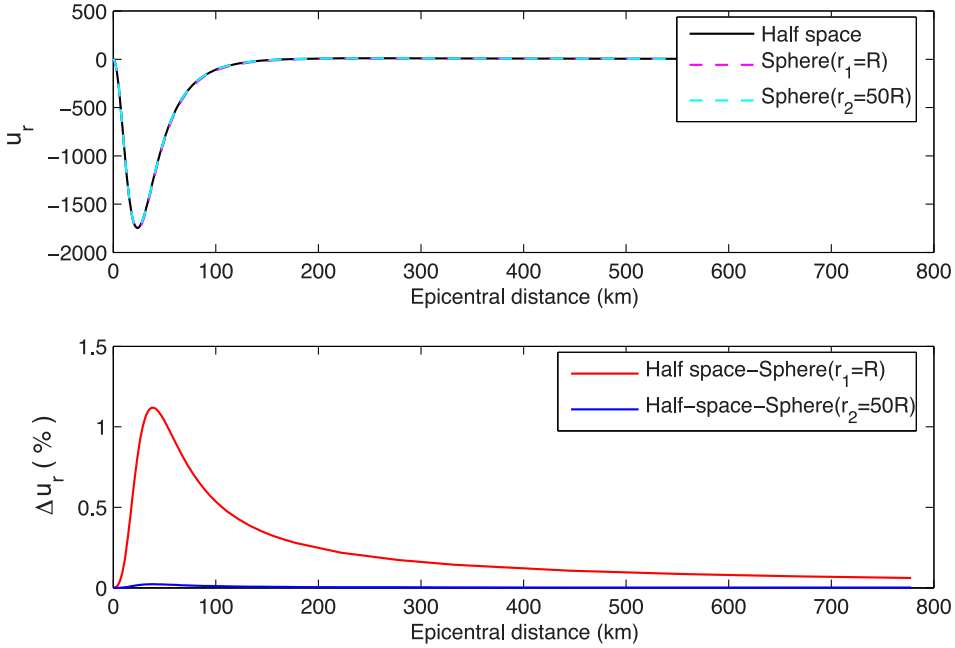

Figure 5. Comparison of the coseismic vertical displacements computed for a half-space, Sphere 1 ($r_1 = R$) and Sphere 2 ($r_2 = 50R$) for a strike-slip point source ($UdS/R^2 = 1$) at a depth of 30 km (the upper panel). The lower panel shows differences of two spheres with respect to the half-space.

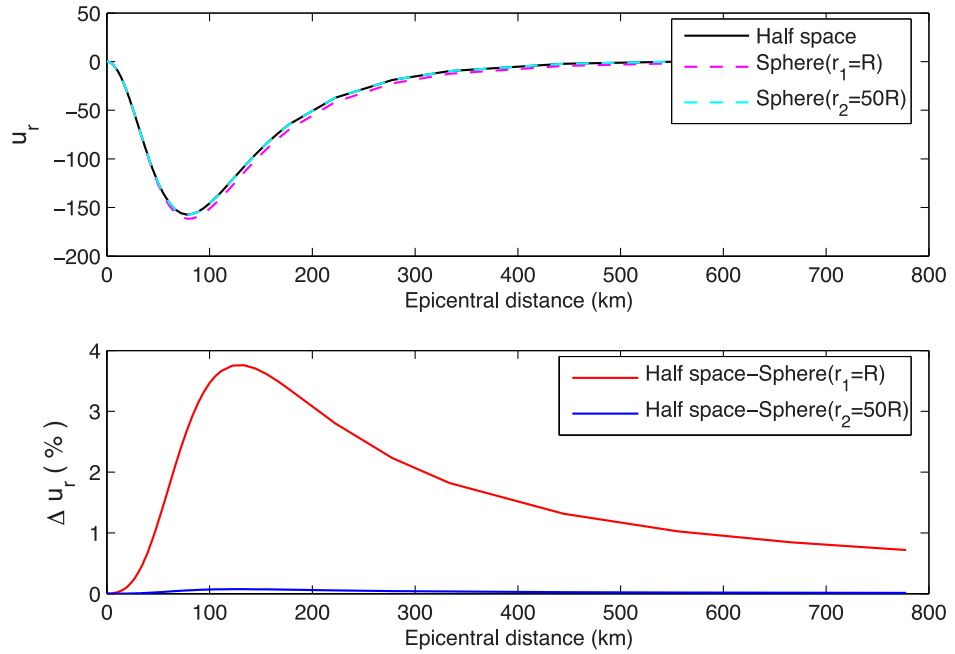

Figure 6. Comparison of the coseismic vertical displacements computed for a half-space, Sphere 1 ($r_1 = R$) and Sphere 2 ($r_2 = 50R$) for a strike-slip point source ($UdS/R^2 = 1$) at a depth of 100 km (the upper panel). The lower panel shows differences of two spheres with respect to the half-space.

The above results are very similar to those given by Pollitz (1996) and Nostro *et al.* (1999) who claimed that the curvature effect is generally less than 2 per cent when the epicentral distance is less than 100 km for strike-slip line, rift line and thrust line sources. However, our results clearly show that the curvature effect depends on the source depth, and deeper sources tend to exhibit a larger curvature effect. For example, the curvature effect can reach be as much as 30 per cent when the source depth is 600 km.

5.2 Curvature effect on the far-field deformations

The relative error obtained by (28) varies smoothly as the epicentral distance increases, because the value of $|\boldsymbol{u}^{(r_1)}|_{\max}$ is a non-zero constant. However, the definition of (28) does not reflect the true curvature effect at an observing point in the far field. For instance, we consider a strike-slip source at depth of 30 km, the maximum coseismic radial displacement Green's function appears at epicentral distance of

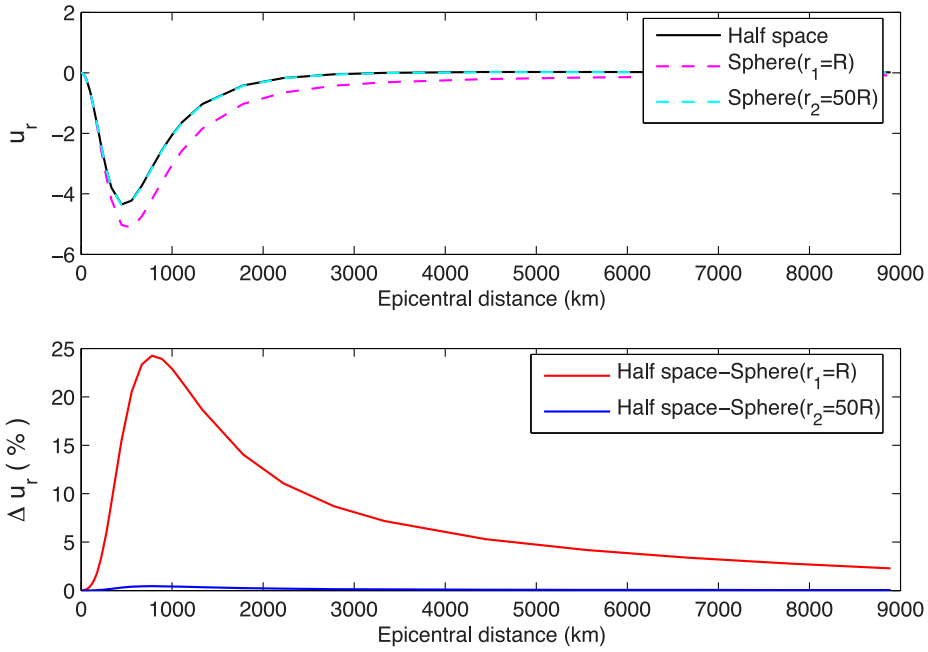

Figure 7. Comparison of the coseismic vertical displacements computed for a half-space, Sphere 1 ($r_1 = R$) and Sphere 2 ($r_2 = 50R$) for a strike-slip point source ($UdS/R^2 = 1$) at a depth of 600 km (the upper panel). The lower panel shows differences of two spheres with respect to the half-space.

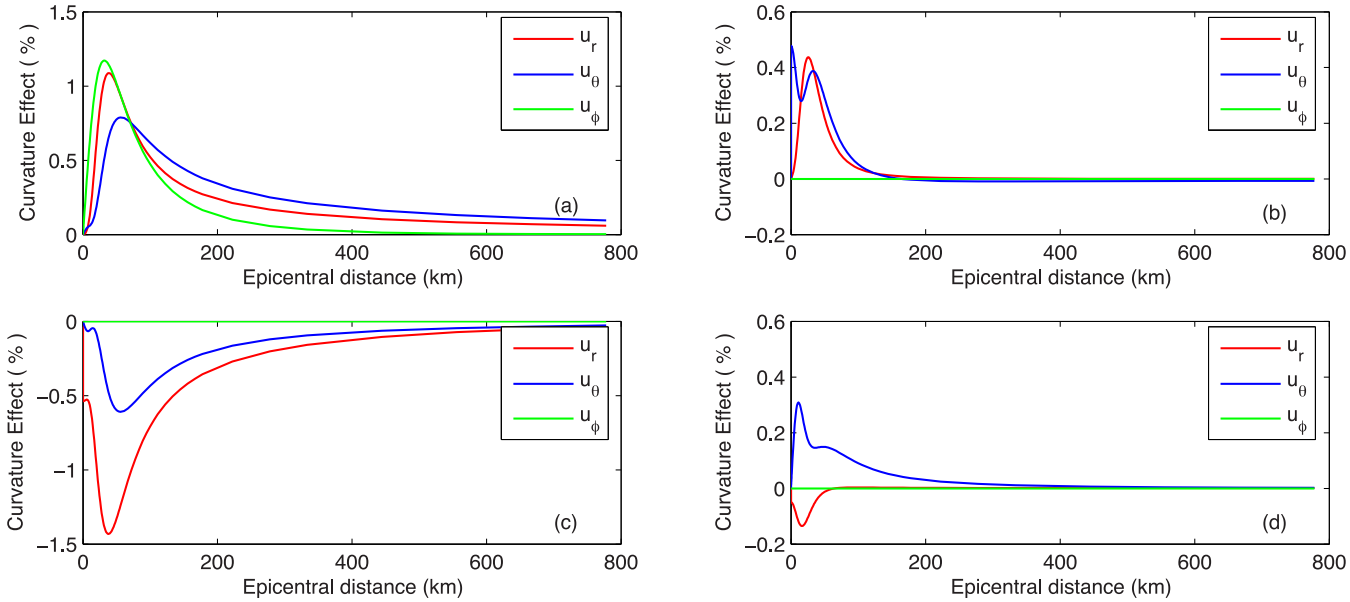

Figure 8. Curvature effect of coseismic displacements caused by the (a) strike-slip, (b) dip-slip, (c) horizontal tensile and (d) vertical tensile, respectively. The source depth is 30 km.

$d = 50$ km and $u^{(r_1)}_{r,\max} = 500$ cm. The coseismic displacements for the two spheres appear at epicentral distance of $d = 500$ km, $u^{(r_1)}_r = 10$ cm and $u^{(r_2)}_r = 16$ cm, respectively. Then, the relative error (curvature effect) calculated by (28) gives $\varepsilon = 1.2$ per cent. The difference at $d = 500$ km is 6 cm, which cannot be simply described by 1.2 per cent, instead it should be 60 per cent if we observe the relative error at the observing point.

Therefore, to reasonably observe the curvature effect, we should consider the curvature effect and define the relative error by

$$\gamma = \frac{\left|\boldsymbol{u}^{(r_2)}\right| - \left|\boldsymbol{u}^{(r_1)}\right|}{\left|\boldsymbol{u}^{(r_1)}\right|} \tag{29}$$

where $|\boldsymbol{u}^{(r_1)}|$ is the value at the observing point, instead of $|\boldsymbol{u}^{(r_1)}|_{\max}$. When $|\boldsymbol{u}^{(r_1)}|$ is zero, the relative error goes to infinity. In this case, we may avoid the point in practical computation.

According to (29), we compute the relative error (curvature effect) of the far-field coseismic displacements for the two spheres, for a strike-slip source at depth of 30 and 600 km, respectively. The results, depicted in Fig. 11, show that the curvature effect defined by (29)

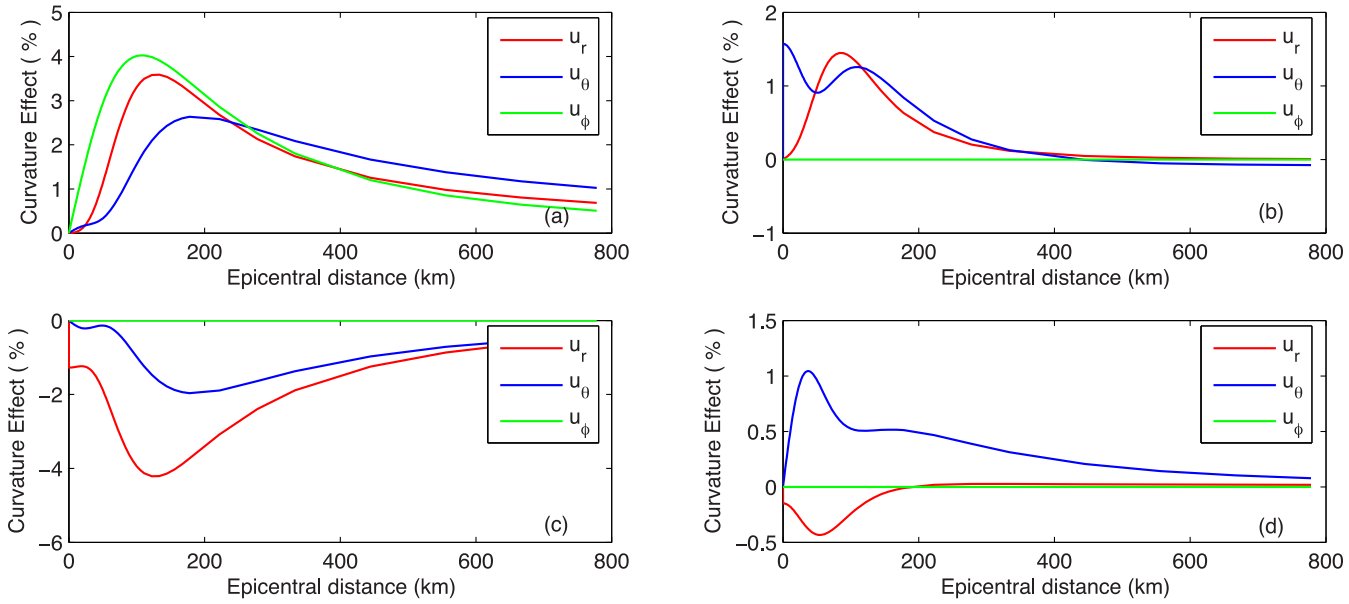

Figure 9. Curvature effect of coseismic displacements caused by the (a) strike-slip, (b) dip-slip, (c) horizontal tensile and (d) vertical tensile, respectively. The source depth is 100 km.

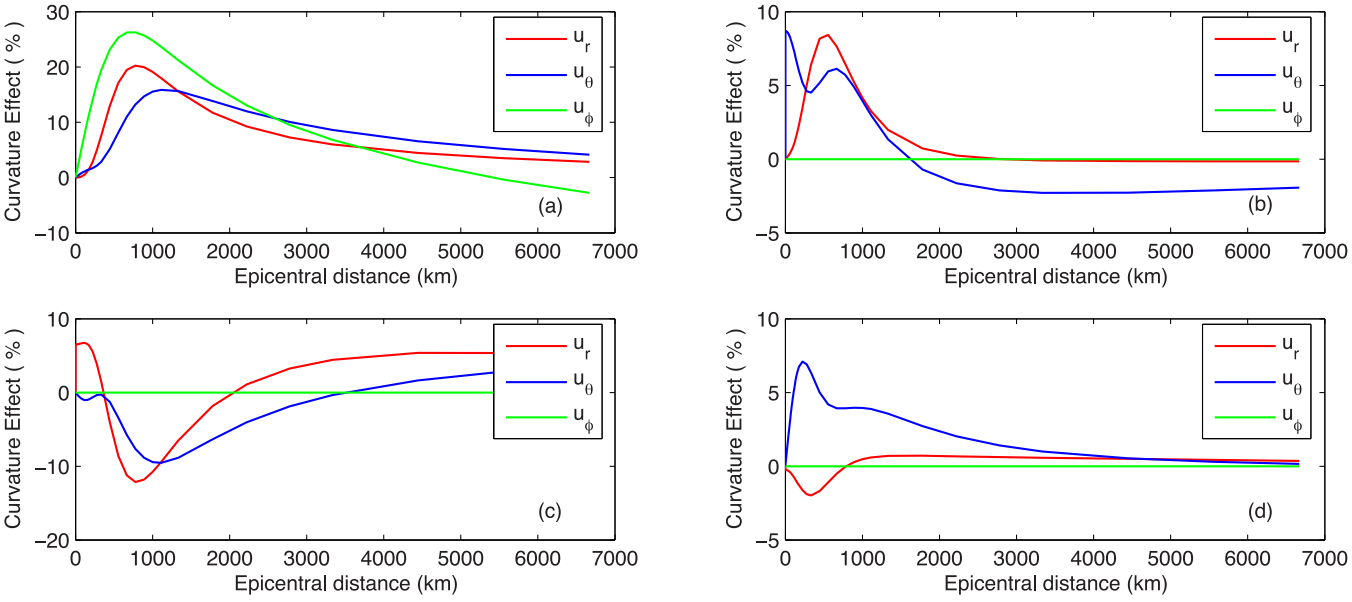

Figure 10. Curvature effect of coseismic displacements caused by the (a) strike-slip, (b) dip-slip, (c) horizontal tensile, and (d) vertical tensile, respectively. The source depth is 600 km.

is very large. The difference in the vertical displacement component for depth of 30 km reaches over 50 per cent in the far field; while the relative error in the vertical displacement for depth of 600 km becomes larger and larger as the epicentral distance increases. The curvature effects for other types of sources are similar in magnitude to those shown in Fig. 11.

6 CURVATURE EFFECT FOR THE MOON

This new scheme can be used to calculate the curvature effect of any planet, not only the earth. Our research indicates that the curvature effect is also related to the sphere radius (except for the epicentral distance), source type and source depth. In this section, we discuss the curvature effect for a smaller sphere, the Moon, with a radius of $r = 0.27R$. Using the same computing scheme, we compute the curvature effect by Moonquakes at depths of 30, 100 and 600 km. The curvature effect is defined by eq. (28), error relative to the maximum displacement, and results in relationships that are illustrated in Figs 12–14 for the three depths. Figs 12–14 show that the maximum curvature effect reaches 4.5 per cent, 17 per cent and 70 per cent, for the source depths of 30, 100 and 600 km, respectively. Therefore, the curvature effect of the Moon is much larger than that of Earth. Because the Earth's radius is 3–4 times larger than the Moon, but the curvature effect of the Moon is also 3–4

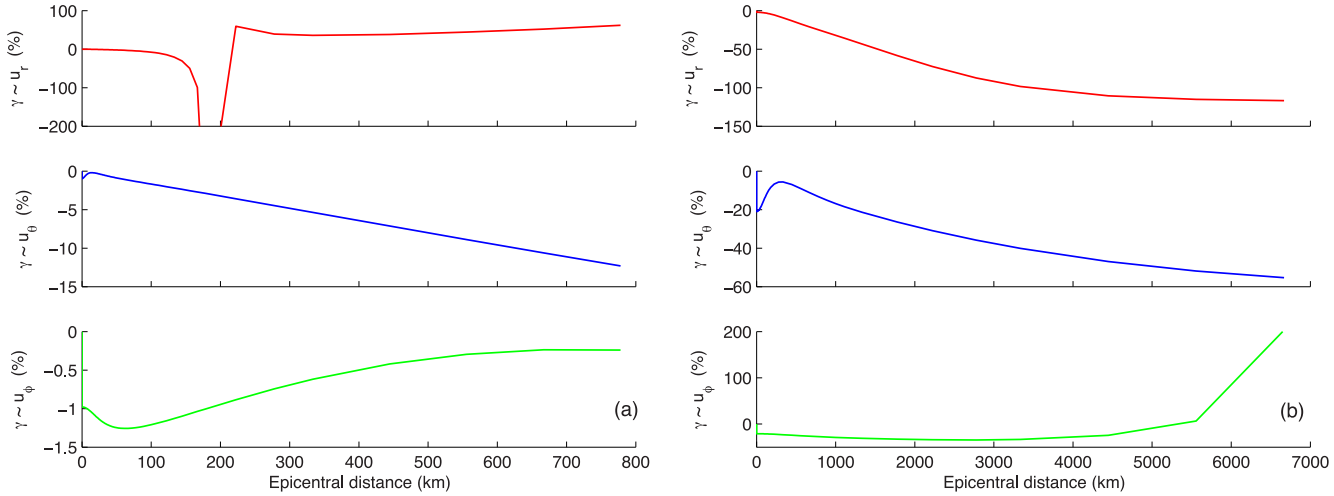

Figure 11. Curvature effect of coseismic displacements caused by strike-slip source. The source depth is (a) 30 km and (b) 600 km.

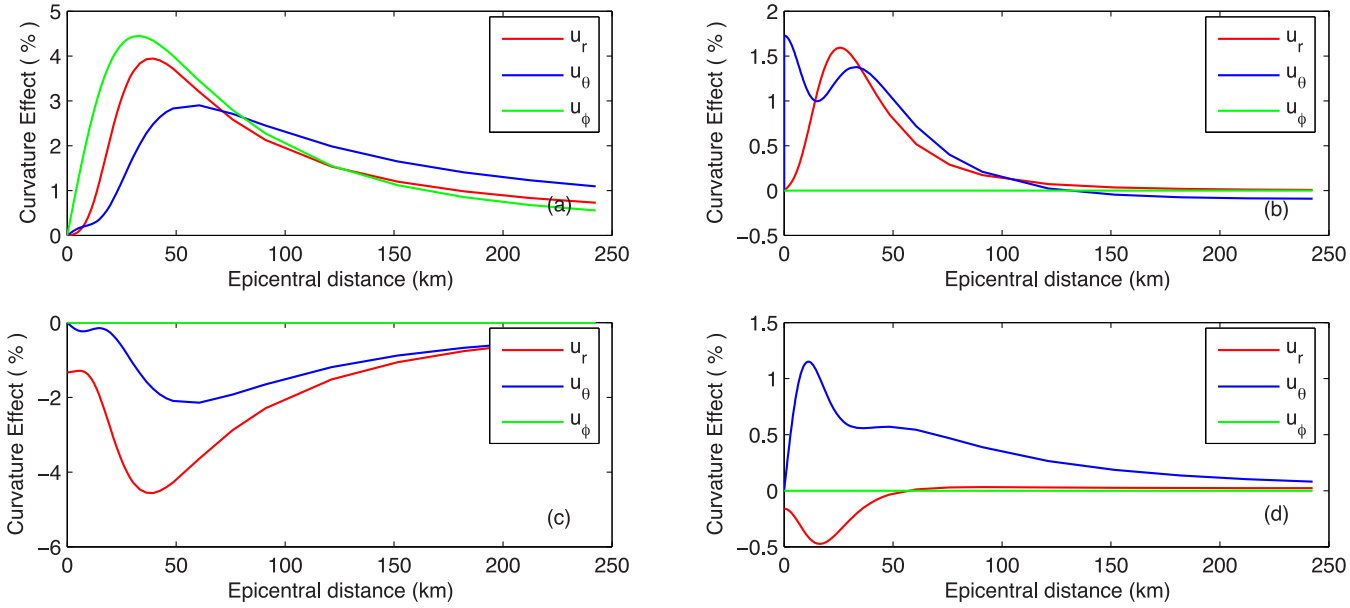

Figure 12. Curvature effect of the Moon, caused by (a) strike-slip, (b) dip-slip, (c) horizontal tensile and (d) vertical tensile, respectively. The source depth is 30 km.

times larger than Earth (considering the same source), then we can estimate the curvature effect for another planet using the ratio of planet's radius to the Earth's radius.

7 DISCUSSION AND CONCLUSIONS

In this study, we propose a new method to investigate the earth's curvature effect on coseismic deformation, by consideration of two homogeneous spheres with different radii. We derive analytical solutions for a homogeneous sphere without gravity. Comparing the analytical solutions of these two spheres, we then estimate the curvature effect and avoid any numerical problems. We find that the difference between a half-space and a large sphere is sufficiently small, so that the method has been proven to be feasible and valid. Then, we use the larger sphere (50 times larger than the earth) instead of the half-space model.

We calculate the coseismic displacements $\boldsymbol{u}(r, \theta, \varphi)$ of four independent sources at various depths for the two spheres. Then, we compare the difference of the coseismic displacements of the two spheres, and obtain the curvature effect. We found that the curvature effect depended on the source type and increased with the source depth in the near field. Generally, the curvature effects of the strike-slip and horizontal tensile sources were larger in the near field. The maximum effect is no more than 5 per cent for strike-slip and horizontal tensile source when the source depth is within 100 km, but about 1.5 per cent for the other sources. This is similar but larger than that given by Pollitz (1996). We also found that the maximum effect was about 30 per cent for a strike-slip source at depths of 600 km, but less than 10 per cent for dip-slip and vertical tensile sources.

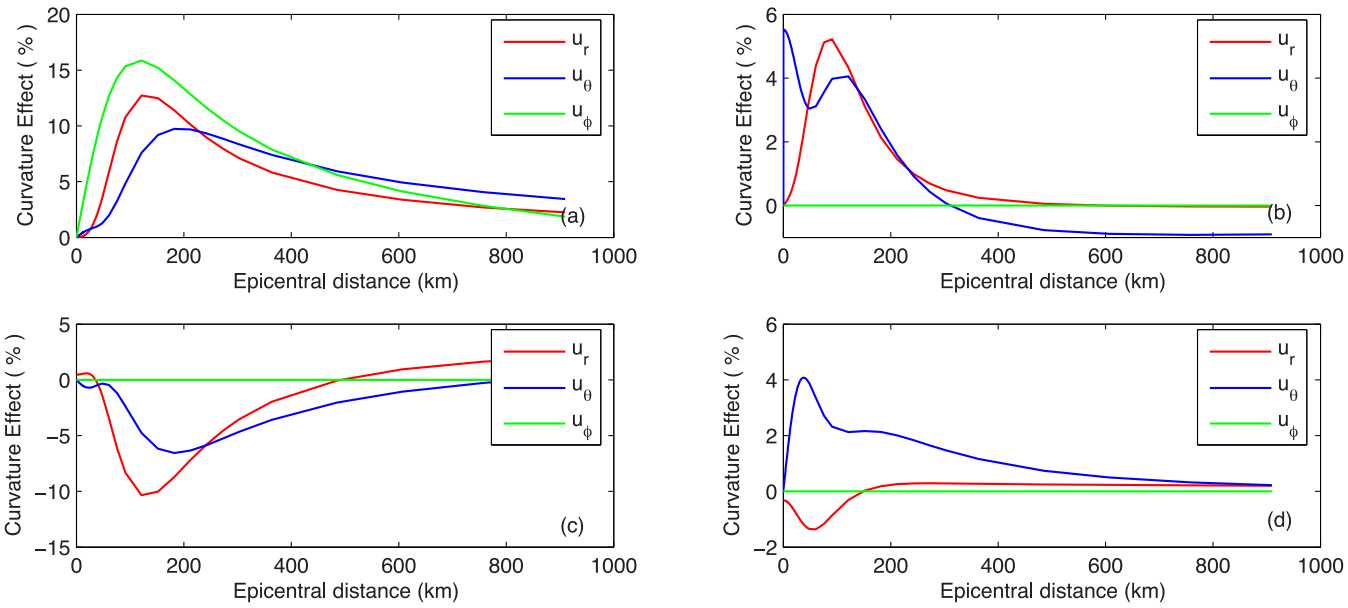

Figure 13. Curvature effect of the Moon, caused by (a) strike-slip, (b) dip-slip, (c) horizontal tensile and (d) vertical tensile, respectively. The source depth is 100 km.

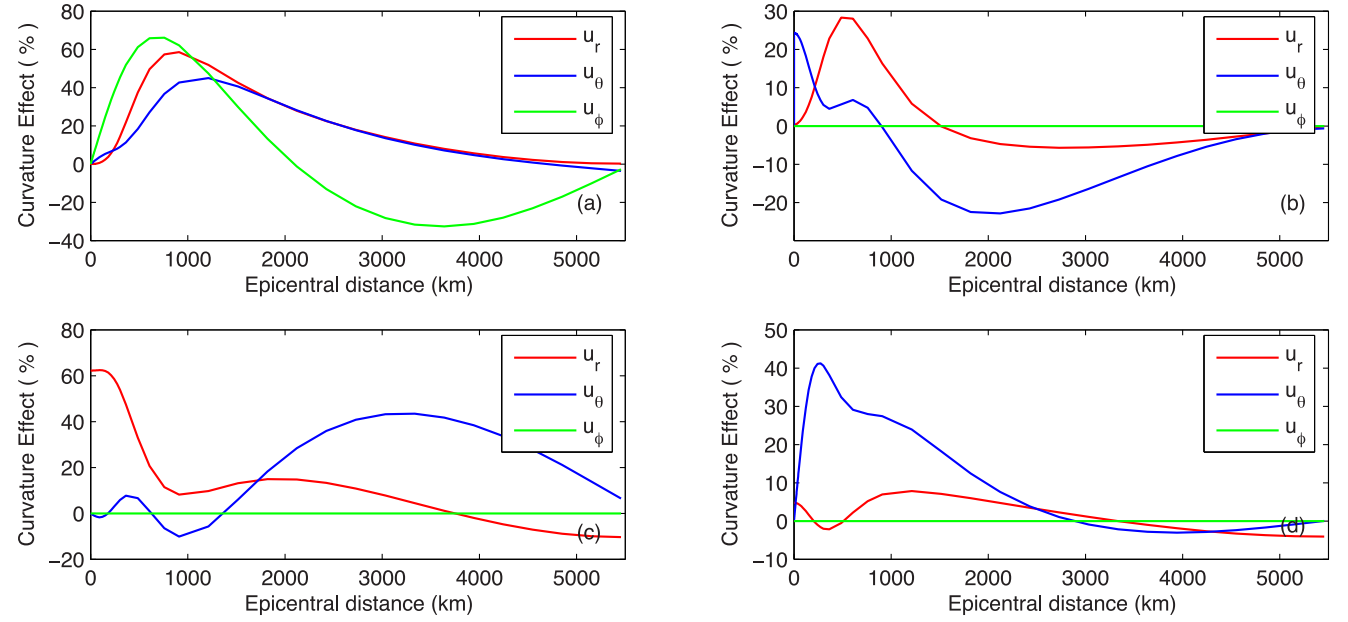

Figure 14. Curvature effect of the Moon, caused by (a) strike-slip, (b) dip-slip, (c) horizontal tensile, and (d) vertical tensile, respectively. The source depth is 600 km.

We consider two definitions including the curvature effect relative to the maximum coseismic displacement and the effect compared to the observing point, to observe the curvature effect. Different definitions result in large discrepancies. For a far-field application, the latter definition is considered most reasonable.

For a smaller sphere (i.e. the Moon), the curvature effect is larger and ratio of the smaller sphere's radius to the earth's radius is inversely related.

The curvature effect is considered to be small compared to the layer effect 25 per cent (Sun & Okubo 2002); however, our study indicates that the curvature effect is also very large for a deep seismic source and if we consider the definition of the effect relative to the observing point. The results of this study must be considered when inverting a fault slip model using far-field displacement because the relative error (curvature effect) is very large.

ACKNOWLEDGEMENTS

This research was supported financially by the National Natural Science Foundation of China (Nos 41331066, 41174063, 41474059 and 41574021), China Postdoctoral Science Foundation funded project (No. 119103S268) and by the CAS/CAFEA International Partnership Program for creative research teams (No. KZZD-EW-TZ-19), as well as the SKLGED foundation (SKLGED2014-1-1-E).

REFERENCES

Alterman, Z., Jarosch, H. & Pekris, C.L., 1959. Oscillation of the Earth, *Proc. R. Soc. Lond.,* **A252,** 80–95.

Ben-Menahem, A. & Israel, M., 1970. Effects of major seismic events on the rotation of the Earth, *Geophys. J. R. astr. Soc.,* **19,** 367–393.

Ben-Menahem, A. & Singh, S.J., 1968. Eigenvector expansions of Green's dyads with applications to geophysical theory, *Geophys. J. R. astr. Soc.,* **16,** 417–452.

Ben-Menahem, A., Singh, S.J. & Solomon, F., 1969. Static deformation of a spherical earth model by internal dislocations, *Bull. seism. Soc. Am.,* **59,** 813–853.

Dong, J., Sun, W., Zhou, X. & Wang, R., 2014. Effects of Earth's structure, gravity and curvature on coseismic deformation, *Geophys. J. Int.,* **199,** 1442–1451.

Dziewonski, A.M. & Anderson, D.L., 1981. Preliminary reference Earth model, *Phys. Earth planet. Inter.,* **25,** 297–356.

Gilbert, F. & Dziewonski, A.M., 1975. An application of normal mode theory to the retrieval of structural parameters and source mechanisms from seismic spectra, *Phil. Trans. R. Soc. Lond., A,* **278,** 187–269.

Love, A.E.H., 1911. *Some Problem of Geodynamics,* Cambridge Univ. Press.

Melini, D., Cannelli, V., Piersanti, A. & Spada, G., 2008. Post-seismic rebound of a spherical Earth: new insights from the application of the Post-Widder inversion formula, *Geophys. J. Int.,* **174,** 672–695.

Nostro, C., Piersanti, A., Antonioli, A. & Spada, G., 1999. Spherical vs. flat models of coseismic and postseismic deformations, *J. geophys. Res.,* **104,** 13 115–13 134.

Okada, Y., 1985. Surface deformation due to shear and tensile faults in a half-space, *Bull. seism. Soc. Am.,* **75,** 1135–1154.

Piersanti, A., Spada, G., Sabadini, R. & Bonafede, M., 1995. Global post-seismic deformation, *Geophys. J. Int.,* **120,** 544–566.

Pollitz, F.F., 1996. Coseismic deformation from earthquake faulting in a layered spherical Earth, *Geophys. J. Int.,* **125,** 1–14.

Saito, M., 1967. Excitation of free oscillations and surface waves by a point source in a vertically heterogeneous Earth, *J. geophys. Res.,* **72,** 3689–3699.

Singh, S.J. & Ben-Menahem, A., 1969. Deformation of a homogeneous gravitating sphere by internal dislocations, *Pageoph,* **76,** 17–39.

Sun, W., Okubo, S., Fu, G. & Araya, A., 2009. General formulations of global co-seismic deformations caused by an arbitrary dislocation in a spherically symmetric Earth model—applicable to deformed Earth surface and space-fixed, *Geophys. J. Int.,* **177,** 817–833.

Sun, W., 2003. Asymptotic theory for calculating deformations caused by dislocations buried in a spherical earth—geoid change, *J. Geod.,* **77,** 381–387.

Sun, W., 2004a. Asymptotic solution of static displacements caused by dislocations in a spherically symmetric Earth, *J. geophys. Res.,* **109**(B5), B05402, doi:10.1029/2003JB002793.

Sun, W., 2004b. Short Note: Asymptotic theory for calculating deformations caused by dislocations buried in a spherical earth—gravity change, *J. Geod.,* **78,** 76–81.

Sun, W. & Okubo, S., 1993. Surface potential and gravity changes due to internal dislocations in a spherical Earth—I. Theory for a point dislocation, *Geophys. J. Int.,* **114,** 569–592.

Sun, W. & Okubo, S., 2002. Effects of earth's spherical curvature and radial heterogeneity in dislocation studies-for a point dislocation, *Geophys. Res. Lett.,* **29**(12), 1605, doi:10.1029/2001GL014497.

Takeuchi, H. & Saito, M., 1972. Seismic surface waves, *Meth. Comput. Phys.,* **11,** 217–295.

Tanaka, T., Okuno, J. & Okubo, S., 2006. A new method for the computation of global viscoelastic post-seismic deformation in a realistic earth model (I)—Vertical displacement and gravity variation, *Geophys. J. Int.,* **164,** 273–289.

Wang, R., 1999. A simple orthonormalization method for stable and efficient computation of Green's functions, *Bull. seism. Soc. Am.,* **89,** 733–741.

Wang, R., 2005. The dislocation theory: a consistent way for including the gravity effect in (visco)elastic plane-earth models, *Geophys. J. Int.,* **161,** 191–196.

Wang, R., Martin, F.L. & Roth, F., 2003. Computation of deformation induced by earthquakes in a multi-layered elastic crust-FORTRAN programs EDGRN/EDCMP, *Comput. Geosci.,* **29,** 195–207.

Wang, R., Lorenzo-Martin, F. & Roth, F., 2006. PSGRN/PSCMP—a new code for calculating co- and post-seismic deformation, geoid and gravity changes based on the viscoelastic-gravitational dislocation theory, *Comput. Geosci.,* **32**(4), 527–541.